Journal of Molecular Graphics and Modelling 72 (2017) 156–167

Contents lists available at ScienceDirect

Journal of Molecular Graphics and Modelling

journal homepage: www.elsevier.com/locate/JMGM

# Computational exploration of regioselectivity and atmospheric lifetime in $NO_3$-initiated reactions of $CH_3OCH_3$ and $CH_3OCH_2CH_3$

Jin-Ting Ye, Feng-Yang Bai, Shao-Qing Shi, Xiu-Mei Pan*

*Institute of Faculty of Chemistry, National & Local United Engineering Lab for Power Battery Northeast Normal University, 130024 Changchun, People's Republic of China*

ARTICLE INFO

*Article history:*
Received 31 July 2016
Received in revised form
20 December 2016
Accepted 3 January 2017
Available online 6 January 2017

*Keywords:*
Transition state
Branching ratio
Atmospheric lifetime

ABSTRACT

The $NO_3$-initiated reactions of $CH_3OCH_3$ and $CH_3OCH_2CH_3$ have been investigated by the BHandHLYP method in conjunction with the 6–311G(d,p) basis set. Thermodynamic and kinetic data are further refined using the comparatively accurate CCSD(T) method. According to the values of reaction enthalpies ($\Delta H^{\theta}_{r,298}$) and reaction Gibbs free energies ($\Delta G^{\theta}_{r,298}$) from $CH_3OCH_2CH_3$ with $NO_3$ system, we find that H-abstraction pathway from the α-$CH_2$ group is more exothermic. It is further confirmed by the calculated C—H bond dissociation energy of $CH_3OCH_2CH_3$ molecule. All the rate constants, computed through means of canonical variational transition state with small-curvature tunneling correction, are fitted to the three-parameter expressions $k_1 = 1.54 \times 10^{-23} T^{3.34} \exp(-1035.53/T)$ and $k_2 = 3.55 \times 10^{-26} T^{4.31} \exp(-281.24/T)$ $cm^3$ $molecule^{-1}$ $s^{-1}$ and branching ratios are computed over the temperature range 200–600 K. The branching ratios are also discussed. The atmospheric lifetimes of $CH_3OCH_3$ and $CH_3OCH_2CH_3$ determined by the $NO_3$ radical are about 270 and 29 days, respectively.



## 1. Introduction

In recent years, more and more volatile organic compounds (VOCs) are detected in the atmosphere [1–4]. The VOCs, such as alcohols, ethers, aldehydes, ketones and esters, are the key atmospheric species which have important contribution as the organic components of atmospheric aerosol and are emitted from both natural and anthropogenic sources. The ethers are considerable parts of VOCs, and the introduction of ether linkage —O— may lead to an even greater reactivity. Ethers are mostly removed in the atmosphere by their wide usage as fuel additive and industrial solvents [5,6]. The VOCs are involved in numerous events in the troposphere: in addition to wet and dry deposition, they can undergo photolysis and oxidative degradation initiated by OH, $NO_3$, and $O_3$. For most of the VOCs, reaction with the hydroxyl radicals is the dominant degradation process during the daytime [7]. On the contrary, the $NO_3$ has been identified and measured by long path spectroscopic techniques to have an average concentration as $5 \times 10^8$–$2 \times 10^9$ molecule $cm^{-3}$ in the nighttime atmosphere [8,9]. Therefore, in the last years, attention has been paid to the $NO_3$ night-time reactivity in urban zones with a large concentration of ethers. The $NO_3$ radicals contribute to the oxidation of ethers and to the formation of $HNO_3$ which is also related to particulate formation and harmful health effects. In addition, reactions of $NO_3$ with biogenic hydrocarbons are particularly efficient and are responsible for the production of organic nitrates and secondary organic aerosols [10–12].

The compounds of $CH_3OCH_3$ and $CH_3OCH_2CH_3$ are typical ethers. The H-abstraction reaction channels of $CH_3OCH_3$ and $CH_3OCH_2CH_3$ with $NO_3$ radicals can be shown as follows:

$$CH_3OCH_3 + NO_3 \rightarrow CH_2OCH_3 + HNO_3 \quad (R1)$$

$$CH_3OCH_2CH_3 + NO_3 \rightarrow CH_2OCH_2CH_3 + HNO_3 \quad (R2)$$

$$CH_3OCH_2CH_3 + NO_3 \rightarrow CH_3OCHCH_3 + HNO_3 \quad (R3)$$

$$CH_3OCH_2CH_3 + NO_3 \rightarrow CH_3OCH_2CH_2 + HNO_3 \quad (R4)$$

Langer et al. [13] first studied rate constant for reaction of $CH_3OCH_3$ with $NO_3$ at 295 K ($(2.60 \pm 1.10) \times 10^{-16}$ $cm^3$ $molecule^{-1}$ $s^{-1}$) using FTIR spectroscopy in a reactor equipped with White optics in experiment. Chen et al. measured the total rate constants by means of the relative rate method, with the results (in $cm^3$ $molecule^{-1}$ $s^{-1}$) of $(1.07 \pm 0.10) \times 10^{-16}$ and $(7.81 \pm 0.36) \times 10^{-16}$ for $CH_3OCH_3$ and $CH_3OCH_2CH_3$ with $NO_3$ radicals at 298 K, respectively [14]. Moreover, Chen et al. computationally explored potential energy surfaces for the $NO_3$ radical reactions, and the rate constants of

* Corresponding author.
*E-mail address:* panxm460@nenu.edu.cn (X.-M. Pan).

http://dx.doi.org/10.1016/j.jmgm.2017.01.002
1093-3263/

$k_1$ and $k_2$ were calculated according to the transition state theory (TST) at 298 K. Meanwhile, the canonical variational transition state with small-curvature tunneling correction (VTST-ISPE) [15] can more accurately obtain a sufficiently wide temperature range of practical interest, branching ratio, and atmospheric lifetimes of title reactions. VTST-ISPE is also widely applied in previously researches [16–18]. Therefore, it is necessary to compare the rate constants of $k_1$ and $k_2$ computed by TST and VTST-ISPE methods. On the one hand, theoretical studies on the extrapolation of temperature dependence of rate constants expand the understanding

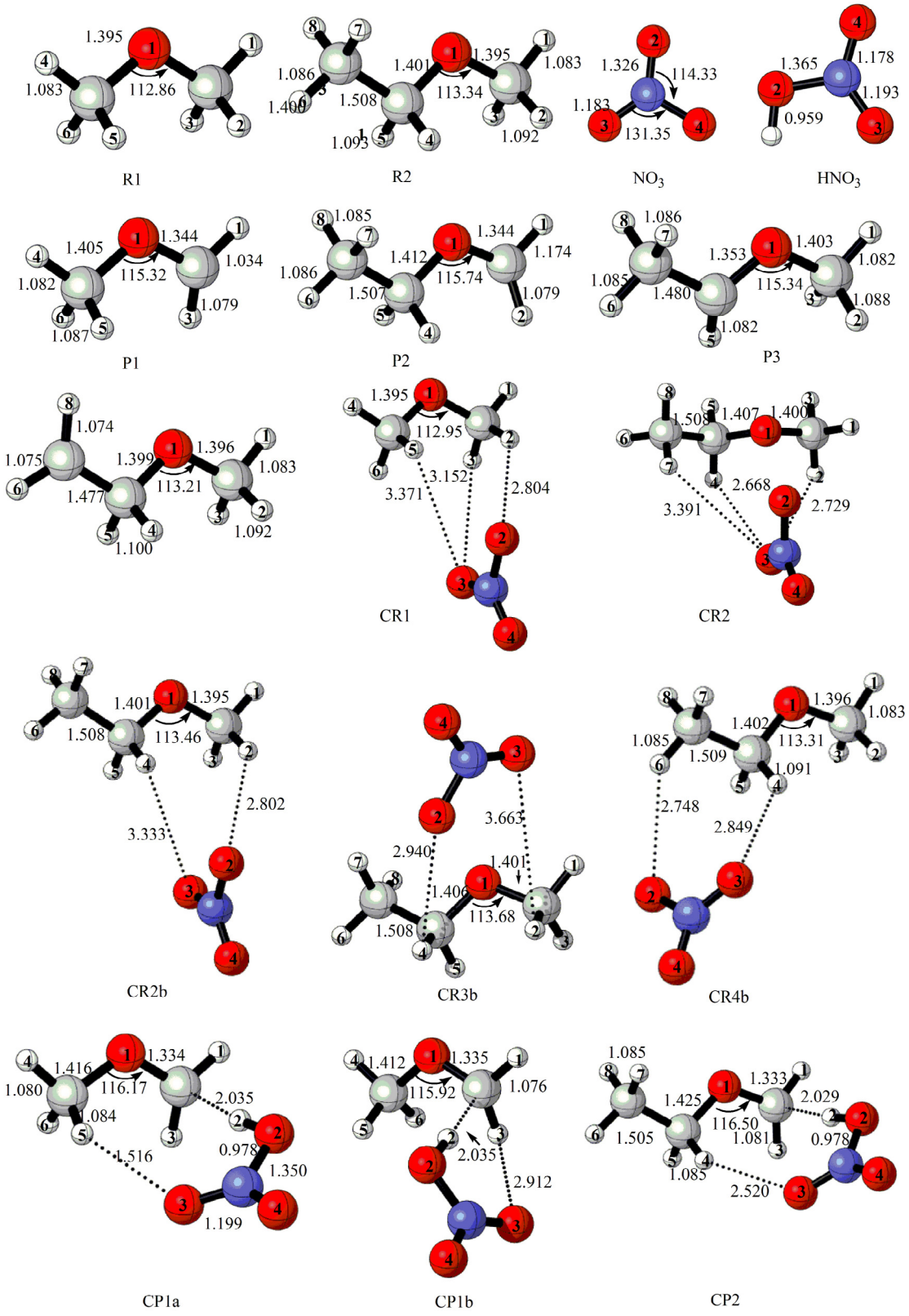


**Fig. 1.** Optimized geometries of the reactants, products, transition states, and complexes at the BHandHLYP/6-311G(d,p) level. Bond lengths (angles) are in angstrom (degree).

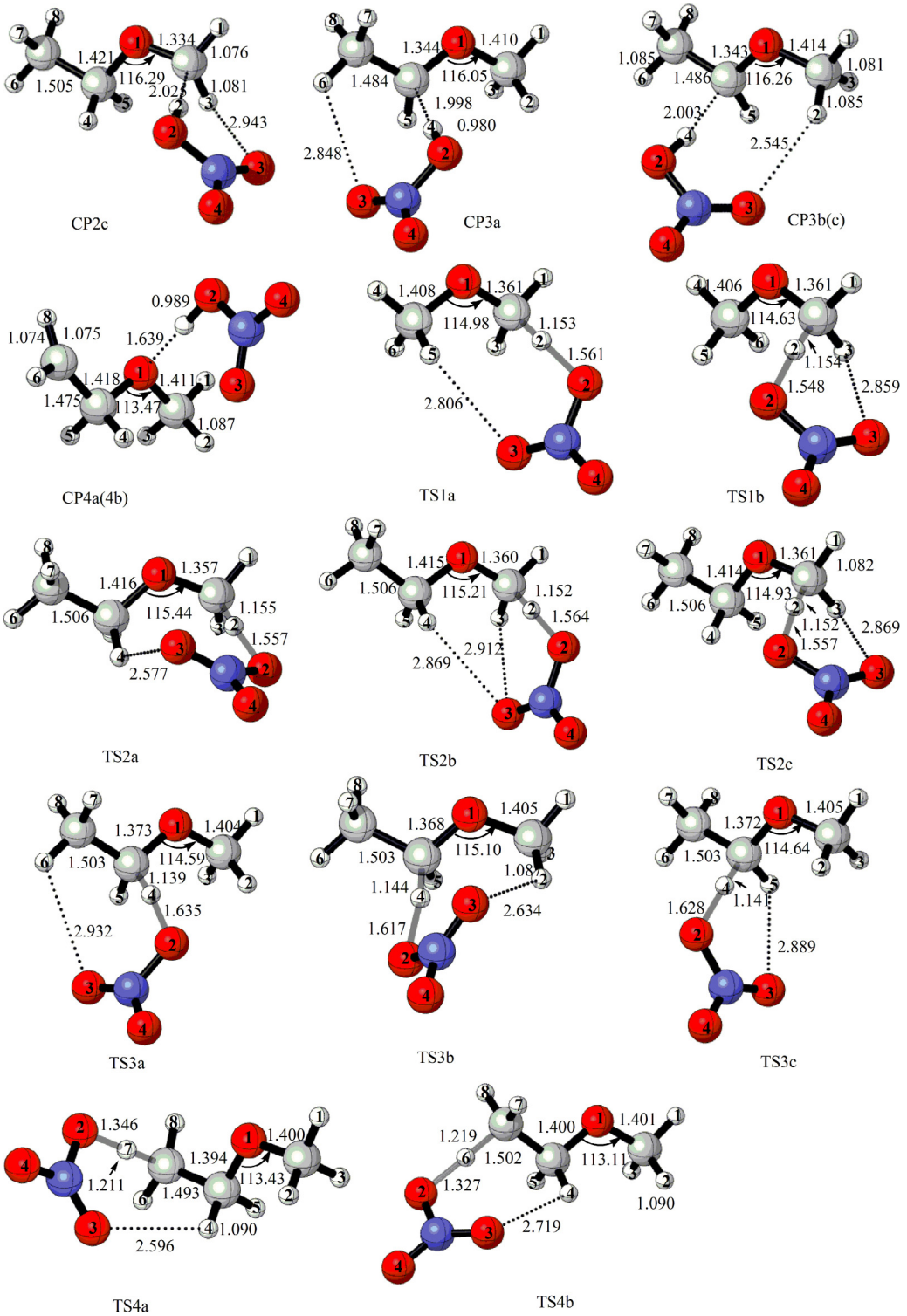


**Fig. 1.** (*Continued*).

of the reaction mechanisms. On the other hand, they can testify the experimental data already published in this field and provide a new explanation for a regioselectivity behavior of this kind of H-abstraction processes.

In the study, density functional theory (DFT) calculation is introduced into the reaction mechanism of $CH_3OCH_3$ and $CH_3OCH_2CH_3$ with $NO_3$ radicals. The dual-level direct dynamics method is employed to study the kinetic nature of the title reactions over a wide temperature range of 200–600 K. Each H-abstraction reaction channels (R1-R4) can proceed in more than one way (Scheme 1). To be more specific, the different interactions between oxygen atom (3O) of the $NO_3$ radical and hydrogen atoms in $CH_3OCH_3$ and $CH_3OCH_2CH_3$ molecules lead to multiple channels. Furthermore, the reaction enthalpies ($\Delta H^{\theta}_{r,298}$), reaction Gibbs free energies ($\Delta G^{\theta}_{r,298}$), and C—H bond dissociation energy ($D^{\theta}_{298}$) are computed at the CCSD(T)//BHandHLYP/6-311G(d,p) level of theory. The branching ratios and atmospheric lifetimes are calculated at the

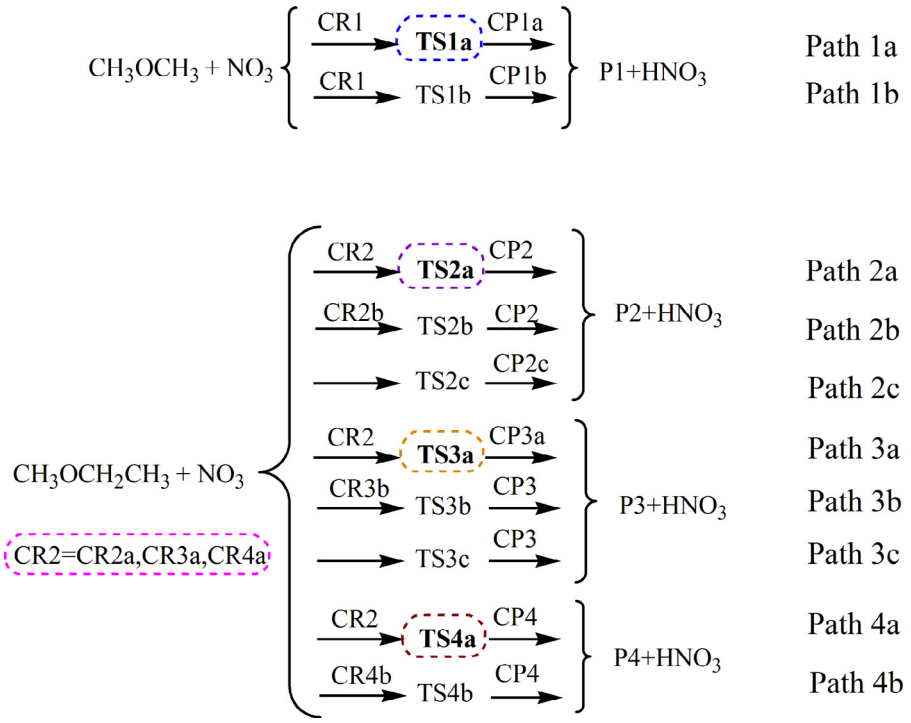


**Scheme 1.** H-abstraction pathways for the reactions $CH_3OCH_3$ and$CH_3OCH_2CH_3$ by $NO_3$ radicals.

dynamics level of the variational transition state theory (VTST) with interpolated single-point energies (ISPE). The theoretical results are discussed and compared with available experimental results.

## 2. Methodology

All the geometrical structures were optimized at the BHandHLYP/6-311G(d,p) [19] level of theory under Gaussian 09 program package [20]. The method was known to be accurate for predicting result in the similar reaction systems [21–24]. Besides, zero-point energies (ZPE) of all the species were calculated at the same level of theory. In order to obtain potential energy surface, single-point energies of optimized geometries were refined using the CCSD(T) [25] method with the same basis set. Galano et al. have proposed that the $T_1$ diagnostic seems not a settled issue to judge multireference character in CCSD(T) wave function. $T_1$ diagnostic probably the most frequently used model among all available tests, which gives a qualitative assessment of the significance of non-dynamical (or static) correlation. Literature information has been proposed that $T_1$ values $\geq$0.02 for closed-shell and 0.045 for open-shell indicate a significant multireference character [26,27]. However, in this work, the $T_1$ values are smaller than 0.02 for closed-shell systems and smaller than 0.045 for open-shell systems, suggesting that the multireference character is not a problem. But it has been reported that these threshold values are not rigorously defined and can be system- and method-dependent.

All rate constant calculations are carried out through the POLYRATE-Version 9.7 program [28]. The theoretical rate constants over the wide temperature range of 200–600 K and activation energies are calculated using the canonical variational transition state theory (CVT) [29,30] including small curvature tunneling correction (SCT) [31,32] method proposed by Truhlar and co-workers. Canonical variational transition state theory rate constants, $k^{CVT}(T)$, at fixed temperature ($T$) by minimizing the generalized transition state theory rate constant, $k^{GT}(T,s)$, with respect to the dividing surface at $s$ is expressed as

$$k^{CVT}(T,s) = \min k^{GT}(T,s) \quad (1)$$

where, $k^{GT}$ for temperature $T$ and dividing surface at $s$ is that

$$k^{\mathrm{GT}}(T,S) = K\frac{\sigma k_B T Q^{\mathrm{GT}(T,S)}}{h\Phi^{\mathrm{R}}(T)}\mathrm{e}^{-V_{\mathrm{MEP}(s)}/k_{\mathrm{B}}T} \quad (2)$$

In this equation, $\kappa$ is the tunneling factor, $\acute{o}$ is the symmetry factor; $s$ is the location of the generalized transition state on the IRC; $h$ is Planck's constant; $\beta$ equals $(k_BT)^{-1}$ where $k_B$ is Boltzmann's constant; and $Q^{GT}$ and $Q^R$ are partition functions for the generalized transition state and reactants, respectively. To take tunneling effect into consideration, the CVT rate constant is multiplied by the small-curvature tunneling (SCT) approximation, which is denoted as $k^{CVT/SCT}(T)$. The values $<S^2>$, vibrational frequencies and the limited experimental data [33–36] of the reactants, complexes, transition states, and products, are given in Table 1. As illustrated in Table 1, the doublet range from 0.755 to 0.765 at the BHandHLYP/6-311G(d,p) level before annihilation. After spin annihilation for the doublet species, the value of $<S^2>$ is nearly 0.750 at the same level of theory, so the spin contamination is not severe [37,38].

## 3. Results and discussion

### 3.1. Electronic structures of the stationary points

For the channels (R1a, R1b, R2a, R3a, R3b, R3d, R4a, and R4b), there are weak hydrogen-bonded complexes formed at the entrance and exit channels. The reaction begins with the barrierless formation of a pre-reaction complex (designated by CR) in the entrance of each channel in Fig. 1. Two moieties of the CR complex ($CH_3OCH_3$ and $CH_3OCH_2CH_3$ with $NO_3$) are held together by a hydrogen bond, which is formed between the hydrogen atom of the ethers and the oxygen atom of the nitrate radical. The same pre-reactant complex (CR2) exists for the main H-abstraction channels (R2a, R3a, and R4a) of reaction $CH_3OCH_2CH_3$ with $NO_3$. The single

**Table 1**
Frequencies (Experimental values are in parentheses) ($cm^{-1}$) and $<s^2>$ values of the reactants, products, transition states, and complexes for the title reactions calculated at the BHandHLYP/6-311G(d,p) level.

| species | Frequencies | $<s^2>$ |
|---|---|---|
| $CH_3OCH_3$ | 212(203),[a] 251(242),[a] 425(418),[a] 999(958),[a] 1172(1102),[a] 1208(1150),[a] 1242(1179),[a] 1271(1227),[a] 1322(1244),[a] 1518(1452),[a] 1535(1452),[a] 1544(1464),[a] 1549(1464),[a] 1551(1464),[a] 1573(1464),[a] 3050(2817),[a] 3063(2817),[a] 3100(2925),[a] 3102(2952),[a] 3202(2996),[a] 3203(2996)[a] | 0.0 |
| $CH_3OCH_2CH_3$ | 115, 215, 273, 297, 481, 853, 909, 1077, 1161, 1212, 1225, 1246, 1295, 1353, 1452, 1490, 1533, 1537, 1541, 1554, 1560, 1589, 3046, 3062, 3074, 3104, 3121, 3191, 3197, 3202 | 0.0 |
| $NO_3$ | 428(368),[b] 703, 832(758),[c] 966(1050),[d] 1455, 1781(1492)[b] | 0.0 |
| $HNO_3$ | 505, 642, 733, 839, 1026, 1412, 1472, 1887, 3911 | 0.0 |
| TS1a | 376*i*, 26, 57, 72, 121, 149, 239, 413, 482, 597, 719, 839, 1002, 1005, 1103, 1180, 1206, 1225, 1307,1367, 1439, 1450, 1522, 1542, 1548, 1553, 1760, 1920, 3097, 3104, 3163, 3221, 3233 | 0.763 |
| TS1b | 360*i*, 18, 48, 73, 106, 164, 290, 375, 444, 585, 722, 839, 1005, 1008, 1112, 1197, 1210, 1239, 1296, 1373, 1409, 1449, 1520, 1542, 1551, 1553, 1768, 1909, 3090, 3108, 3151, 3228, 3232 | 0.763 |
| TS2a | 398*i*, 29, 39, 64, 104, 126, 238, 275, 299, 374, 488, 594, 716, 841, 849, 901, 1003, 1083, 1105, 1165, 1211, 1231, 1278, 1357, 1385, 1418, 1444, 1457, 1494, 1535, 1538, 1554, 1570, 1748, 1894, 3087, 3095, 3126, 3146, 3198, 3207, 3217 | 0.763 |
| TS2b | 375*i*, 18, 41, 53, 79, 119, 199, 263, 305, 443, 497, 595, 719, 839, 843, 901, 1001, 1082, 1095, 1172, 1185, 1227, 1287, 1347, 1359, 1436, 1450, 1455, 1493, 1535, 1537, 1552, 1574, 1762, 1931, 3093, 3104, 3125, 3132, 3198, 3203, 3220 | 0.763 |
| TS2c | 344*i*, 17, 38, 55, 87, 104, 237, 283, 303, 372, 486, 588, 721, 839, 848, 902, 1004, 1084, 1112, 1168, 1213, 1234, 1275, 1351, 1361, 1412, 1449, 1455, 1493, 1534, 1535, 1554, 1577, 1768, 1939, 3084, 3108, 3120, 3126, 3198, 3204, 3225 | 0.763 |
| TS3a | 218*i*, 34, 38, 65, 96, 132, 175, 215, 298, 306, 487, 595, 713, 836, 845, 917, 1000, 1087, 1168, 1180, 1203, 1222, 1272, 1318, 1382, 1441, 1460, 1477, 1533, 1536, 1543, 1552, 1557, 1767, 2152, 3080, 3088, 3124, 3142, 3194, 3212, 3225 | 0.762 |
| TS3b | 281*i*, 21, 50, 71, 107, 139, 173, 207, 287, 303, 488, 594, 712, 833, 840, 919, 1001, 1085, 1164, 1177, 1198, 1221, 1277, 1315, 1404, 1440, 1463, 1479, 1529, 1534, 1541, 1553, 1555, 1759, 2061, 3068, 3092, 3124, 3160, 3194, 3209, 3229 | 0.762 |
| TS3c | 226*i*, 10, 41, 65, 93, 119, 194, 203, 298, 302, 491, 594, 712, 838, 863, 920, 999, 1084, 1161, 1167, 1199, 1223, 1273, 1298, 1384, 1445, 1462, 1481, 1529, 1536, 1541, 1551, 1555, 1767, 2113, 3082, 3092, 3123, 3149, 3193, 3207, 3226 | 0.762 |
| TS4a | 1413*i*, 21, 42, 85, 101, 129, 212, 248, 295, 467, 488, 549, 729, 815, 838, 884, 905, 1021, 1086, 1132, 1190, 1226, 1231, 1282, 1314, 1334, 1396, 1452, 1466, 1503, 1535, 1543, 1552, 1573, 1792, 3013, 3071, 3111, 3122, 3168, 3214, 3253 | 0.764 |
| TS4b | 1520*i*, 35, 47, 56, 97, 109, 151, 232, 276, 412, 513, 566, 734, 814, 835, 861, 948, 1014, 1070, 1127, 1209, 1212, 1244, 1277, 1293, 1348, 1355, 1452, 1469, 1523, 1540, 1541, 1560, 1590, 1800, 3068, 3077, 3121, 3123, 3171, 3212, 3256 | 0.765 |
| CR1 | 16, 27, 41, 44, 50, 53, 221, 264, 426, 439, 703, 832, 963, 1000, 1172, 1209, 1242, 1272, 1323, 1451, 1519, 1535, 1545, 1549, 1550, 1572, 1776, 3048, 3061, 3102, 3104, 3203, 3204 | 0.756 |
| CR2b | 16, 27, 35, 38, 46, 47, 119, 216, 272, 297, 439, 481, 703, 832, 854, 909, 963, 1077, 1161, 1213, 1224, 1245, 1296, 1352, 1450, 1452, 1490, 1533, 1537, 1540, 1553, 1559, 1587, 1775, 3041, 3059, 3078, 3106, 3121, 3191, 3197, 3202 | 0.756 |
| CR2 | 34, 49, 76, 91, 113, 122, 165, 218, 280, 302, 480, 548, 706, 836, 853, 902, 997, 1073, 1158, 1205, 1213, 1243, 1291, 1357, 1441, 1454, 1490, 1531, 1534, 1544, 1554, 1560, 1581, 1776, 3068, 3081, 3115, 3124, 3135, 3195, 3200, 3210 | 0.756 |
| CR3b | 39, 42, 61, 87, 98, 126, 167, 222, 280, 310, 479, 556, 707, 833, 851, 903, 993, 1072, 1159, 1204, 1213, 1244, 1291, 1355, 1437, 1452, 1489, 1529, 1535, 1548, 1553, 1558, 1581, 1784, 3064, 3077, 3096, 3125, 3127, 3194, 3206, 3230 | 0.757 |
| CR3d | 10, 35, 50, 62, 87, 104, 159, 214, 274, 301, 480, 541, 704, 833, 850, 903, 987, 1074, 1158, 1206, 1213, 1242, 1290, 1354, 1439, 1453, 1490, 1533, 1534, 1542, 1551, 1556, 1582, 1787, 3062, 3076, 3092, 3126, 3127, 3196, 3206, 3213 | 0.756 |
| CR4b | 16, 19, 24, 32, 40, 49, 117, 215, 272, 298, 430, 481, 703, 832, 857, 908, 963, 1076, 1160, 1213, 1224, 1247, 1295, 1354, 1448, 1452, 1491, 1531, 1537, 1541, 1544, 1560, 1593, 1770, 3041, 3060, 3089, 3103, 3120, 3190, 3193, 3203 | 0.756 |
| CP1a | 29, 45, 80, 89, 112, 141, 190, 396, 453, 671, 731, 743, 846, 850, 1002, 1048, 1190, 1223, 1312, 1364, 1463, 1475, 1516, 1546, 1558, 1564, 1863, 3114, 3172, 3194, 3241, 3313, 3491 | 0.755 |
| CP1b | 19, 29, 60, 83, 97, 147, 216, 389, 447, 668, 741, 750, 843, 846, 1010, 1043, 1186, 1220, 1308, 1364, 1464, 1475, 1515, 1546, 1552, 1563, 1867, 3106, 3173, 3178, 3238, 3321, 3499 | 0.755 |
| CP2 | 17, 26, 60, 78, 101, 107, 172, 256, 302, 399, 491, 671, 732, 743, 844, 847, 851, 895, 1048, 1082, 1157, 1227, 1278, 1353, 1362, 1456, 1464, 1474, 1494, 1534, 1540, 1556, 1582, 1862, 3110, 3125, 3172, 3174, 3198, 3205, 3311, 3485 | 0.755 |
| CP2c | 14, 26, 48, 75, 83, 104, 205, 256, 306, 385, 491, 669, 742, 755, 842, 846, 851, 899, 1043, 1085, 1156, 1226, 1274, 1351, 1358, 1455, 1465, 1476, 1491, 1535, 1539, 1554, 1578, 1867, 3102, 3127, 3143, 3178, 3199, 3205, 3320, 3486 | 0.755 |
| CP3a | 30, 35, 58, 83, 91, 114, 173, 180, 244, 304, 492, 671, 726, 742, 790, 847, 930, 1044, 1088, 1112, 1173, 1221, 1243, 1345, 1437, 1464, 1475, 1487, 1527, 1534, 1546, 1555, 1558, 1864, 3076, 3101, 3155, 3166, 3180, 3207, 3234, 3437 | 0.755 |
| CP3 | 24, 41, 71, 85, 96, 107, 154, 183, 229, 304, 491, 672, 729, 743, 772, 846, 926, 1048, 1087, 1105, 1172, 1224, 1242, 1348, 1438, 1466, 1476, 1486, 1521, 1535, 1546, 1559, 1562, 1862, 3076, 3110, 3155, 3177, 3188, 3201, 3237, 3437 | 0.755 |
| CP3d | 19, 29, 65, 86, 91, 131, 149, 183, 229, 301, 493, 667, 737, 741, 762, 845, 928, 1041, 1089, 1111, 1173, 1222, 1242, 1345, 1436, 1460, 1468, 1487, 1520, 1532, 1547, 1555, 1558, 1866, 3076, 3101, 3166, 3167, 3208, 3234, 3479 | 0.755 |
| CP4 | 37, 45, 85, 95, 120, 165, 176, 189, 254, 323, 468, 509, 687, 750, 851, 854, 994, 1018, 1064, 1096, 1157, 1198, 1228, 1279, 1315, 1459, 1468, 1506, 1533, 1538, 1544, 1550, 1567, 1861, 3023, 3102, 3115, 3170, 3221, 3241, 3294, 3356 | 0.755 |
| $CH_3OCH_2$ | 94, 246, 296, 305, 491, 635, 849, 905, 1089, 1154, 1228, 1269, 1337, 1354, 1452, 1489, 1534, 1535, 1555, 1580, 3085, 3123, 3124, 3188, 3194, 3200, 3338 | 0.755 |
| $CH_2OCH_2CH_3$ | 67, 101, 178, 203, 360, 449, 675, 815, 947, 1053, 1130, 1192, 1197, 1225, 1286, 1325, 1442, 1495, 1151, 1518, 1531, 3063, 3088, 3145, 3166, 3177, 3208 | 0.755 |
| $CH_3OCHCH_3$ | 112, 166, 206, 294, 486, 629, 924, 1064, 1122, 1171, 1221, 1245, 1338, 1432, 1482, 1518, 1535, 1542, 1555, 1558, 3054, 3087, 3141, 3146, 3181, 3197, 3218 | 0.755 |
| $CH_3OCH_2CH_2$ | 97, 136, 230, 303, 420, 495, 876, 1000, 1103, 1143, 1224, 1228, 1287, 1299, 1458, 1502, 1533, 1540, 1551, 1571, 2973, 3019, 3060, 3105, 3205, 3240, 3356 | 0.755 |

[a,b,c,d] from Reference [33,34,35,36] respectively.

energy minimum for the $NO_3$ radical predicted by BHandHLYP is a $C_{2v}$ structure with one long (2O—N) and two short O—N bonds. This result agrees with the conclusions formed by Sherrill and co-workers [39] that the DFT functions of BHandHLYP, M05 and M05-2X predict a single energy minimum which is the broken symmetry structure 1L2S. Additionally, the M06-2X function predicts both symmetry breaking structures 1L2S and 1S2L to be minima on the ground state PES of the $NO_3$ radical. Specifically, the B3LYP function predicts a single energy minimum on the ground state PES of the nitrate radical, which is the fully symmetric $D_{3h}$ structure [21]. By constant, the bond (2O—N) is more active than two short bonds for H-abstraction reactions, thus, H-abstraction reactions occur in the oxygen atom (2O) of $NO_3$ radical. Moreover, oxygen

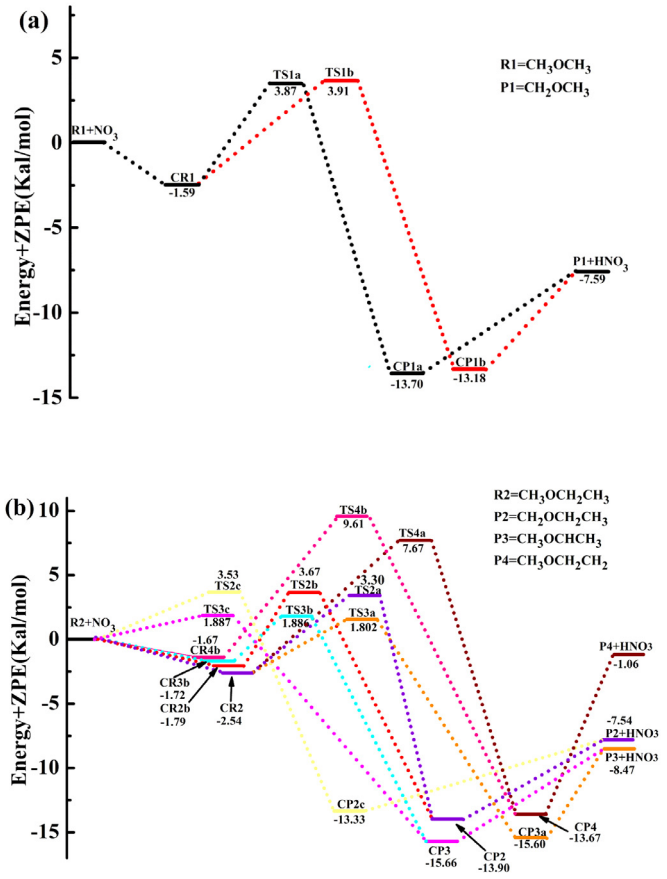


**Fig. 2.** Schematic potential energy surfaces for the title reactions. Relative energies (in kcal/mol) are calculated at the CCSD(T)//BHandHLYP/6-311G(d,p) + ZPE level. (a) For reaction R1, (b) For reactions R2-4.

atom (3O) of the short bond has regioselectivity with different hydrogen atoms in title molecules.

As described in Fig. 1, in all the transition states (TS1a, TS1b, TS2a, TS2b, TS2c, TS3a, TS3b, TS3c, TS3d, TS4a, and TS4b), the breaking C—H bonds are elongated ranging from 4.2% (TS3d) to 10.9% (TS4b) compared with the equilibrium C—H bond in $CH_3OCH_3$ and $CH_3OCH_2CH_3$, whereas the forming O—H bonds are shorten ranging from 27.7% (TS4b) to 41.3% (TS3d) over the equilibrium the O—H bond length in $HNO_3$. The elongation of the breaking bond is smaller than that of the forming bond, indicating that the transition states are reactant-like and the reactions may proceed via early transition states. Besides, the reaction energies of channel R1, R2, R3, and R4 are −7.50, −7.46, −8.28 and −0.73 kcal/mol at the CCSD(T)//BHandHLYP/6-311G(d,p) level of theory, respectively, which agree with the Hammond postulate [40]. The schematic potential energy diagram of the title reactions with the ZPE corrections is plotted in Fig. 2. The total energies of the reactants were set at zero as a reference for the other species.

### 3.2. Reaction mechanism

For channel R1, products $CH_3OCH_2$ and $HNO_3$ are generated via transition state TS1a and TS1b, which are labeled as Path R1a and R1b, respectively. Path R1a and R1b begin with the formation of same pre-reactant complex CR1 (−1.59 kcal/mol), our calculations predict a short bond length of 2.804 Å for the hydrogen-bond of this complex. The product complexes (CP1a and CP1b) are present. The difference of these transition states structure is the regioselectivity of the $NO_3$ radical. In Path R1a, oxygen atom (3O) of the short O—N bond has an interaction with hydrogen atom (5H) which is in the opposite side α-$CH_3$ group of $CH_3OCH_3$, but oxygen atom (3O) attacks on hydrogen atom (3H) of the same carbon in Path R1b. The relative energies of Path R1a (3.87 kcal/mol) and R1b (3.91 kcal/mol) are competitive in Fig. 2a. The numerical result indicates the channel R1a of $NO_3$ radicals attack on hydrogen atoms of α-$CH_3$ group on two sides of ether bond is more favorable.

For channel R2, products $CH_2OCH_2CH_3$ and $HNO_3$ can be obtained via TS2a, TS2b, and TS2c. All paths are labeled as Path R2a, R2b, and R2c, respectively. Paths R2a and R2c begin with the formation of pre-reactant complex CR2a and CR2b (2.54 and 1.79 kcal/mol), respectively. Oxygen atom (3O) of the short O—N bond has an interaction with hydrogen atom (4H) of the $CH_3OCH_2CH_3$ in TS2a (O···H, 2.577 Å). For TS2b, oxygen atom (3O) of short O—N bond has interaction with hydrogen atoms 3H (O···H, 2.912 Å) and 4H (O···H, 2.869 Å), while the oxygen atom (3O) of short O—N bond is toward α-$CH_3$ group in TS2c. Therefore, we can predict that $NO_3$ radicals having interaction with hydrogen atom of α-$CH_2$ site is more favorable than two sides of ether bond and α-$CH_3$ group of $CH_2OCH_2CH_3$. From Fig. 2b, the reaction energies for TS2a, TS2b, and TS2c are quite close, with the values of 3.30, 3.53, and 3.67 kcal/mol, respectively. By constant, the channel containing the α-$CH_3$ site of $CH_3OCH_2CH_3$ with $NO_3$ is lower than the corresponding channel of $CH_3OCH_3$ with $NO_3$. Therefore, it can be concluded that the relative energy will reduce with the addition of a $-CH_2-$ group. The results are in good consistent with similar systems $CH_3OCH_3/CH_3OCH_2CH_3$ and $CH_3OCF_3/CF_3OCH_2CH_3$ with OH radical [16,17,41].

Channel R3 are preceded via H-abstraction from α-$CH_2$ (4H) by the oxygen atom (2O) of long O—N bond. Three pathways have been identified via transition states TS3a, TS3b, and TS3c. The CR3a and CR3b possess 2.54 kcal/mol with hydrogen-bond length 2.668 Å, 1.72 kcal/mol with hydrogen-bond length 2.940 Å, respectively. As described in Fig. 1, we can see that oxygen atom (3O) of the short O—N bond have interactions with hydrogen atom (6H) from β-$CH_3$ site of $CH_3OCH_2CH_3$ in TS3a (O···H, 2.932 Å) which is more stable than hydrogen atoms from α-$CH_3$ (2H), and α-$CH_2$ (5H) in $CH_3OCH_2CH_3$ molecule. The relative energies of Path R3a, R3b, and R3c are 1.802, 1.886 and 1.887 kcal/mol, respectively. The largest difference between any two energies is only 0.85 kcal/mol, indicated that their rate constants will compete with each other.

Channels R4, products $CH_3OCH_2CH_2$ and $HNO_3$ can be obtained via TS4a and TS4b. All paths are preceded via H-abstraction from β-$CH_3$ site by $NO_3$ radical, namely "out–of–plane hydrogen abstraction" (channel 4a) and "in–plane hydrogen abstraction" (channel 4b). There are two pre-reactant complexes CR4a (−2.54 kcal/mol), CR4b (−1.67 kcal/mol) and a product complex CP4 (12.61 kcal/mol). The relative energies of channels R4a and R4b are 7.67 and 9.61 kcal/mol. This well depth indicates the H-abstraction from "out–of–plane" is easier than "in–plane" for β-$CH_3$. Therefore, H-abstraction from α-$CH_2$ region occurs easily because of its lower barrier heights than α-$CH_3$, and β-$CH_3$ sites.

Chen, et al. [14] calculated the barrier height of α-$CH_3$ site for $CH_3OCH_3$ and α-$CH_2$ site, α-$CH_3$ site, and β-$CH_3$ site for $CH_3OCH_2CH_3$ with $NO_3$ radical at the CCSD(T, FC)//BHandHLYP/6-311G(d,p) level, respectively. All frozen core options (FC) meaning are available with this keyword. In this work; the $NO_3$-initiated reactions are analyzed in detail by comparing the competitive Paths of the corresponding H-abstraction sites at CCSD(T)//BHandHLYP/6-311G(d,p) level. For the α-$CH_3$ site in $CH_3OCH_3$; Path R1a (3.87 kcal/mol) and R1b (3.91 kcal/mol) are competitive and simultaneous because of the regioselectivity of the $NO_3$ radical. However; the barrier height of α-$CH_3$ site is 4.34 kcal/mol when frozen core options are considered during the calculation by Chen; et al. For reaction $CH_3OCH_2CH_3$ with $NO_3$ radical; three TS structures have been identified for H-abstraction from the α-$CH_3$ site; three TS structures for α-$CH_2$ site; and two

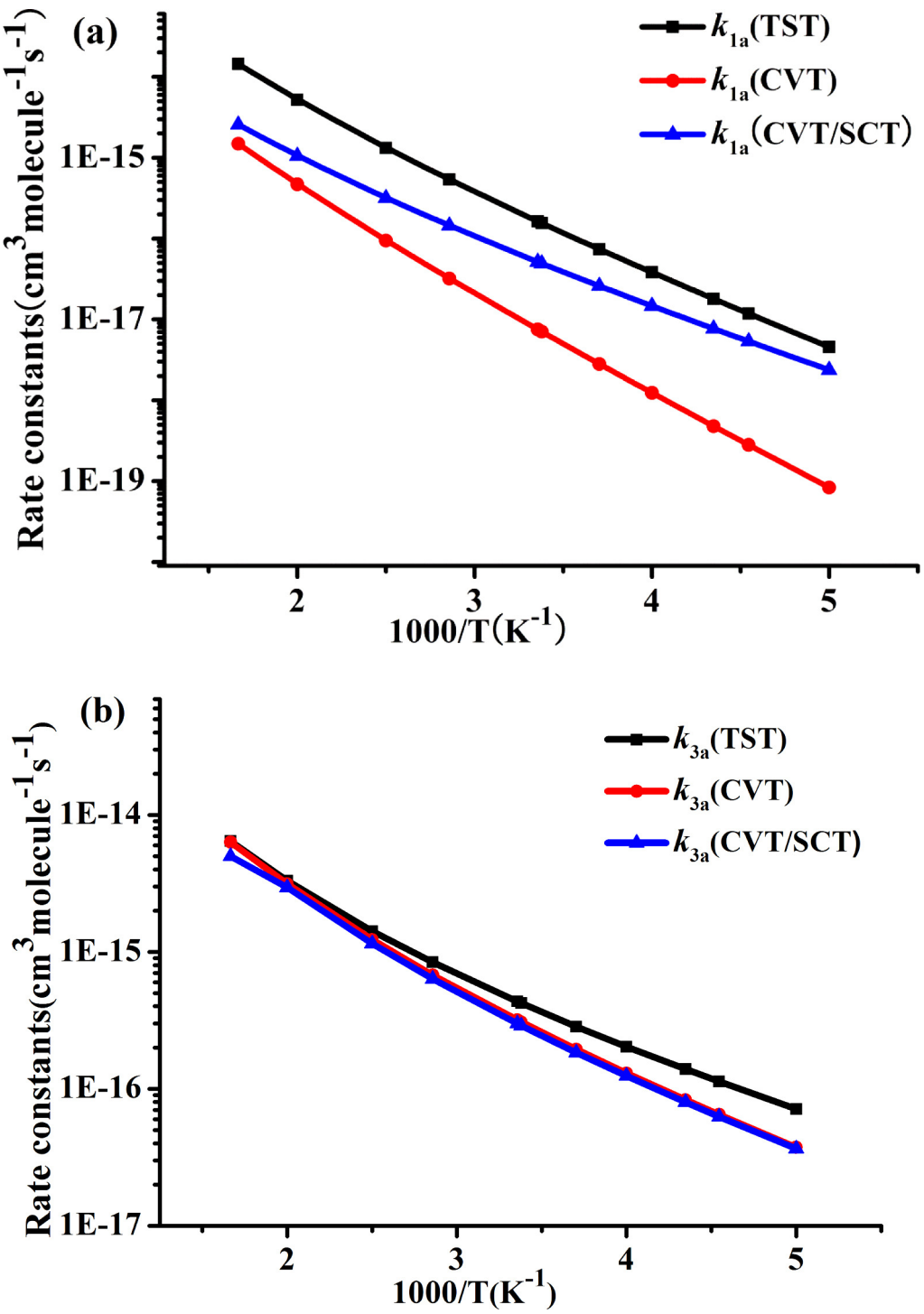


**Fig. 3.** Calculated TST, CVT, and CVT/SCT rate constants as a function of $10^3/T$ for reaction channels R1a and R3a in the temperature range of 200–600 K. (a) For reaction R1a, (b) For reaction R3a.

TS structures for $\beta$-$CH_3$ site in this work. Among all paths from the $\alpha$-$CH_2$ site; the relative energies of TS3a; TS3b; and TS3c are 1.802; 1.886 and 1.887 kcal/mol; within the change of 0.49 kcal/mol compared with frozen core options (2.29 kcal/mol). According to the comparison of methods between CCSD(T) and CCSD(T; FC); the relative energies without frozen core options are lower than these with frozen core options; within the difference from 0.33 to 0.50 kcal/mol for the most favorable paths. Therefore; we can compare the regioselectivity of $NO_3$ radical in H-abstraction reactions and provide a contrast of the energy data between CCSD(T) and CCSD(T; FC) methods.

### 3.3. The enthalpies and the Gibbs free energies

It is well known that accurate values of reaction enthalpies ($\Delta H^{\theta}_{r,298}$), reaction Gibbs free energies ($\Delta G^{\theta}_{r,298}$) and the C—H bond dissociation energies ($D^{\theta}_{298}$) are important parameters to determine the thermodynamic properties and the kinetics of atmospheric processes. From Table 2, the favorable reaction channel

**Table 2**
Reaction enthalpies $\Delta H^{\theta}_{r,298}$ and reaction Gibbs free energies $\Delta G^{\theta}_{r,298}$ for R1-R4 and the bond dissociation energy $D^{\theta}_{298}$ of the C—H in molecules $CH_3OCH_3$ and$CH_3OCH_2CH_3$ at the BHandHLYP/6-311G(d,p) and CCSD(T)//BHandHLYP/6-311G(d,p) levels (kcal/mol).

| | BHandHLYP/6-311G(d,p) | CCSD(T)//BHandHLP/6-311G(d,p) |
|---|---|---|
| $\Delta H^{\theta}_{r,298}$ | | |
| $CH_3OCH_3 + NO_3 \rightarrow CH_3OCH_2 + HNO_3$ (R1a,1b) | −9.20 | −7.50 |
| $CH_3OCH_2CH_3 + NO_3 \rightarrow CH_2OCH_2CH_3 + HNO_3$ (R2a,2b,2c) | −9.21 | −7.46 |
| $CH_3OCH_2CH_3 + NO_3 \rightarrow CH_3OCHCH_3 + HNO_3$ (R3a,3b,3c) | −10.68 | −8.28 |
| $CH_3OCH_2CH_3 + NO_3 \rightarrow CH_3OCH_2CH_2 + HNO_3$ (R4a,4b) | −3.26 | −0.73 |
| $\Delta G^{\theta}_{r,298}$ | | |
| $CH_3OCH_3 + NO_3 \rightarrow CH_3OCH_2 + HNO_3$ (R1a,1b) | −9.29 | −7.59 |
| $CH_3OCH_2CH_3 + NO_3 \rightarrow CH_2OCH_2CH_3 + HNO_3$ (R2a,2b,2c) | −9.33 | −7.58 |
| $CH_3OCH_2CH_3 + NO_3 \rightarrow CH_3OCHCH_3 + HNO_3$ (R3a,3b,3c) | −11.08 | −8.68 |
| $CH_3OCH_2CH_3 + NO_3 \rightarrow CH_3OCH_2CH_2 + HNO_3$ (R4a,4b) | −3.96 | −1.43 |
| $D^{\theta}_{298}$ | | |
| $CH_3OCH_3 \rightarrow CH_3OCH_2 + H$ | 91.65 | 91.51 |
| $CH_3OCH_2CH_3 \rightarrow CH_2OCH_2CH_3 + H$ | 91.64 | 91.55 |
| $CH_3OCH_2CH_3 \rightarrow CH_3OCHCH_3 + H$ | 90.16 | 90.73 |
| $CH_3OCH_2CH_3 \rightarrow CH_3OCH_2CH_2 + H$ | 97.59 | 98.28 |

R3 (−8.28 kcal/mol) is more exothermic than R1 (−7.50 kcal/mol), R2 (−7.46 kcal/mol), and R4 (−0.73 kcal/mol), H-abstraction from α–$CH_2$ group is thermodynamically stable than from —$CH_3$ groups. The values of $\Delta G^{\theta}_{r,298}$ are −7.59 kcal/mol, −7.58 kcal/mol, −8.68 kcal/mol, and −1.43 kcal/mol, respectively, showing that the $NO_3$-initiated reactions of $CH_3OCH_3$ and $CH_3OCH_2CH_3$ are all spontaneous in theory at standard conditions. Thus, R3 is more exothermic and spontaneous in those reactions. The obtained $D^{\theta}_{298}$ value for reaction $CH_3OCH_3$ with $NO_3$ is 91.51 kcal/mol. The α-$CH_2$ site is close to 90.73 kcal/mol lower than α-$CH_3$ (91.55 kcal/mol) and β-$CH_3$ (98.28 kcal/mol) sites of $CH_3OCH_2CH_3$ with $NO_3$ system. Therefore, owing to the lower C—H bond dissociation energy, α-$CH_2$ group is more reactive toward hydrogen abstraction than α-$CH_3$ and β-$CH_3$ groups. This is also reflected in the calculated barrier height for H-abstraction from α-$CH_2$, α-$CH_3$, and β-$CH_3$ sites. Similar conclusions are also observed for $CH_3I$ and $C_2H_5I$ species suggesting that α-$CH_2$ group is found to be more reactive toward hydrogen abstraction by $NO_3$ radicals [42].

### 3.4. Rate constant calculations

Dual-level dynamics calculations are carried out with the VTST-ISPE approach for the reactions of $CH_3OCH_3$ and $CH_3OCH_2CH_3$ with $NO_3$ radical at the CCSD(T)//BHandHLYP/6-311G(d,p) level. As shown in Fig. 2, the mechanism of the title reactions can be described as a two-step, i.e., the first reversible step leads to the reactant complex formation, and the second irreversible step yields the corresponding products. The hypothesis and the method have been presented in detail below and applied successfully to describe the reactions of the free radical with several volatile organic chemicals [43–46]. Detailed discussions are shown below:

$$R_1 + R_2 \underset{k_{-1}}{\overset{k_1}{\leftrightarrow}} R_1 \ldots R_2 \quad \text{step1}$$

$$R_1 \ldots R_2 \overset{k_2}{\rightarrow} P_1 + P_2 \quad \text{step2}$$

$k_1$ is the forward rate constant and $k_{-1}$ is the reverse rate constant in the first step. $k_2$ is equivalent to the second step. According to the steady-state analysis to display the total rate constant:

$$k = \frac{k_1 k_2}{k_{-1} + k_2} \tag{3}$$

As is first pointed by Singleton and Cvetanovic [47] that $k_{-1}$ is much larger than $k_2$, thus $k$ could be rewritten as:

$$k = \frac{k_1 k_2}{k_{-1}} = K_{eq} k_2 \tag{4}$$

where $K$eq is the equilibrium constant between the isolated reactants and the reactant complex. After applying basic statistical thermodynamic principles, $K$eq can be expressed as

$$K_{eq} = \frac{Q_{CR}}{Q_R} \exp\left(\frac{E_R - E_{CR}}{RT}\right) \tag{5}$$

where $Q_{CR}$ and $Q_R$ are the partition functions corresponding to the reactant complex and the isolated reactants, respectively. Under high-pressure conditions, in a unimolecular process, an equilibrium distribution of reactants is established, and the classical TST approach can be applied to calculate $k_2$ (the second step)

$$k_2 = \kappa \frac{k_B T Q_{TS}}{h Q_{CR}} \exp\left(\frac{E_{CR} - E_{TS}}{RT}\right) \tag{6}$$

Where $\kappa$ is the tunneling factor; $k_B$ and $h$ are the Boltzmann and Planck constants, respectively; and $Q_{TS}$ is the TS partition function. The reaction path degeneracy is not included in this expression since the rotational symmetry numbers are already introduced in the calculation of the partition functions. The partition functions are obtained from the rotational constants and the vibrational frequencies of the DFT calculations. The energy differences include the zero-point corrections. Finally, the effected rate constant can be written as

$$k = K_{eq} k_2 = \kappa \frac{k_B T Q_{TS}}{h Q_R} \exp\left(\frac{E_R - E_{TS}}{RT}\right) \tag{7}$$

So the rate constant corresponding to all the studied reaction channels can be analyzed in terms of TST. As in previous works for similar mechanisms [43,44,48,49], we have assumed that in the

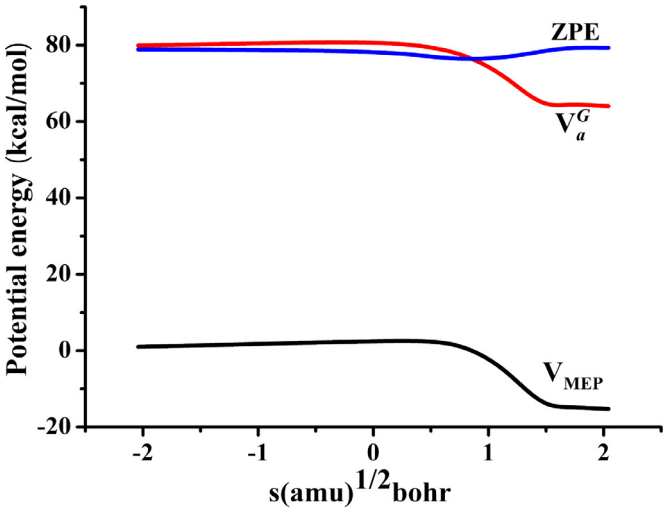


**Fig. 4.** Classical potential energy curve ($V_{MEP}$), ground-state vibrational adiabatic energy curve ($V_a^G$), and zero-point energy curve (ZPE) as functions of $s$ (amu)$^{1/2}$ bohr at the CCSD(T)//BHandHLYP/6-311G(d,p) level for the reaction channel R3a.

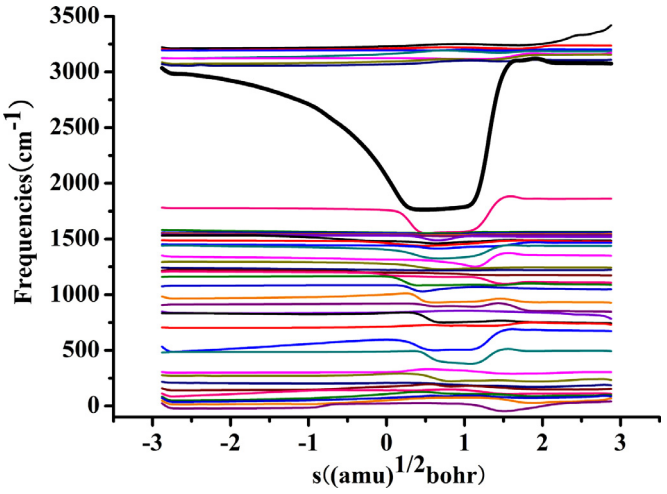


**Fig. 5.** Changes of generalized normal-mode vibrational frequencies as a function of $s$ (amu)$^{1/2}$ bohr at the CCSD(T)//BHandHLYP/6-311G(d,p) level for reaction path R3a.

channel the reactant complex undergoes collisional stabilization; i.e., this reaction step occurs in a high-pressure limit.

The rate constants are evaluated by TST and VTST-ISPE over a wide temperature region from 200 to 600 K for each reaction channels. The TST, CVT, and CVT/SCT rate constants of reaction channels R1a and R3a are presented in Fig. 3a and b, respectively. The variational effect is defined as the ratio between the TST and CVT rate constants and the tunneling effect is the ratio between the CVT/SCT and CVT rate constants. From Fig. 3a, we can see that the gaps exist between rate constants of curves TST and CVT/SCT with CVT rate constants in the whole temperatures, implying that the variational and tunneling effects play major roles in the $NO_3$-initiated reactions of $CH_3OCH_3$. For instance, the ratios between $k^{CVT/SCT}$ and $k^{CVT}$ are 28.4 at 200 K, 6.85 at 298 K, 2.24 at 500 K. This phenomenon can be found in many similar articles investigating the $NO_3$ radical with $CH_3I$ and $C_2H_5I$ species [42]. As shown in Fig. 3b, the variational effect plays a minor role for R3a at low temperatures and become negligible in the high temperatures. However, the CVT and CVT/SCT curves of R3a are coincide exactly and nearly the same with each other over the whole temperature range (200–600 K), indicating that tunneling effect is almost not existing or almost negligible. The following study will further support this view and this phenomenon can be occurred in the similar reaction systems [16,18]. To further understand the title reactions, it is important to compare the variational and tunneling effects of the main paths. From Fig. 3a and b, we can find the gaps of the TST and CVT/SCT with CVT rate constants for $CH_3OCH_2CH_3$ is shrinking than that of $CH_3OCH_3$ system, indicating the variational and tunneling effects will be smaller with the reduce with the addition of a $-CH_2-$ group. Meanwhile, all the TST, CVT and CVT/SCT rate constants have positive temperature dependence.

The kinetic calculations are performed for all H-abstraction reactions using the optimized structures and energies obtained at the BHandHLYP/6-311G(d,p) level. For the reactions involving the reactant complex, the reactant complex is taken into account when we calculated the rate constant. Fig. 4 shows the plots of the classical potential energy curve ($V_{MEP}$), the ground-state vibrational adiabatic energy curve ($\overset{G}{Va}$), and zero-point energy curve (ZPE) as a function of $s$ (amu)$^{1/2}$ bohr at the CCSD(T)//BHandHLYP/6-311G(d,p) level for the advantage channel R3a. According to the expression $\overset{G}{Va} = V_{MEP} + ZPE$ for the effective potential, the $V_{MEP}$ and $\overset{G}{Va}$ curves are similar in shape, and the maxima are closed at the 0.27 (amu)$^{1/2}$ bohr, implying that the variational effect will be small.

The variations on the generalized normal mode vibrational frequencies along the MEP of channel R3a are shown in Fig. 5. The frequencies at about $s = -2.0$ (amu)$^{1/2}$ bohr in the reactant region are associated with the reactant complex, CR3a, and in the product region at about $s = 2$ (amu)$^{1/2}$ bohr, the frequencies are associated with the product complex, CP3a. As the reaction proceeds, most of those frequencies do not change significantly when going from the reactants to the products, but apparently only one generalized vibrational frequency changes dramatically near the saddle point, shown as the solid black line in Fig. 5. This solid black line is called as "reactive mode", which is a typical character for hydrogen transfer reaction [50].

### 3.5. Branching ratios

The theoretical total rate constants $k_1$ ($k_{1a} + k_{1b}$) and $k_2$ ($k_{2a} + k_{2b} + k_{2c} + k_{3a} + k_{3b} + k_{3c} + k_{4a} + k_{4b}$) obtained from the sum of the individual results as well as the available experimental values of title reactions are plotted in Fig. 6. As shown in Fig. 6a, the computed rate constant for R1 is $8.61 \times 10^{-17}$ cm$^3$ molecule$^{-1}$ s$^{-1}$ which is very close to the experimental values $(1.07 \pm 0.10) \times 10^{-16}$ cm$^3$ molecule$^{-1}$ s$^{-1}$ by Chen et al. at 298 K. The similar conclusion can be drawn in the similar reaction system [18]. From Fig. 6b, it is pleasing to observe that our computed rate constant for $k_2$ at 298 K ($6.40 \times 10^{-16}$ cm$^3$ molecule$^{-1}$ s$^{-1}$) is in excellent agreement with the experimental value $(7.81 \pm 0.36) \times 10^{-16}$ cm$^3$ molecule$^{-1}$ s$^{-1}$ and Chen's theoretical value $8.12 \times 10^{-16}$ cm$^3$ molecule$^{-1}$ s$^{-1}$. The total rate constant and individual rate coefficients increase with increasing temperature, which is consistent with the reports regarding the investigation of temperature effect of some similar reaction $CH_3OCH_3$ and $CH_3OCH_2CH_3$ with OH radicals [16,17].

In order to further study the products distribution and proportion of hydrogen abstraction reactions $CH_3OCH_3$ and $CH_3OCH_2CH_3$ with $NO_3$ radical, the temperature dependence of the $k_{1a}/k_1$, $k_{1b}/k_1$, $k_{2a}/k_a$ $k_{2b}/k_2$, $k_{2c}/k_2$, $k_{3a}/k_2$, $k_{3b}/k_2$, $k_{3c}/k_2$, $k_{4a}/k_2$, and $k_{4b}/k_2$ and branching ratios are exhibited in Fig. 7a (7b). As seen in Fig. 7a, both of the channels (R1a and R1b) are important in the total reactions and the contribution of R1b becomes larger while the contribution of R1a decreases with the temperature increasing. From Fig. 7b, it is seen that four channels from $\alpha$–$CH_2$ group (R3a, R3b, and R3c)

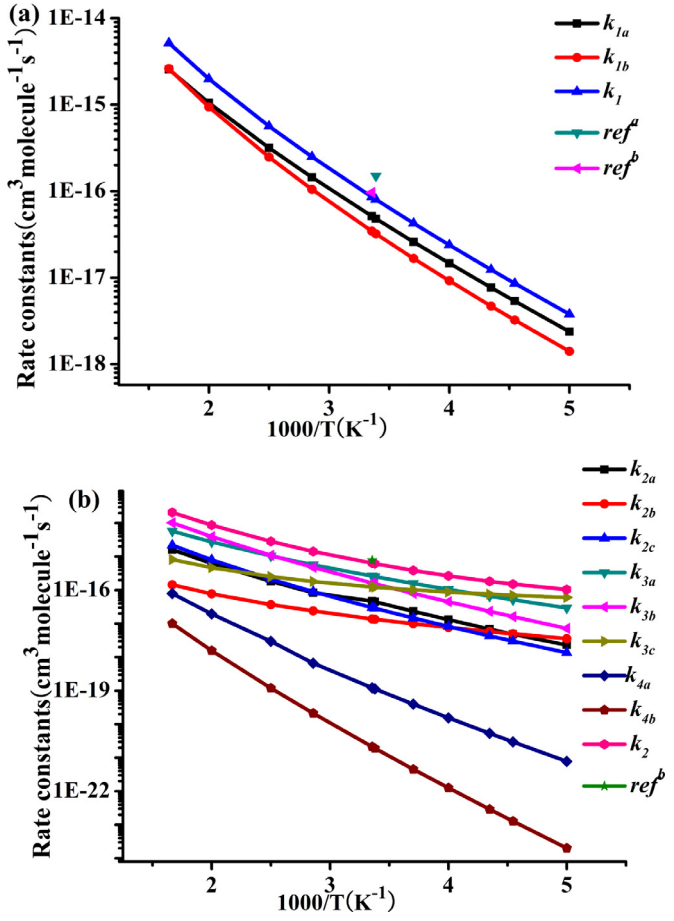


**Fig. 6.** Computed rate constants for the reaction pathways of $CH_3OCH_3 + NO_3$ ($k_{1a}$ and $k_{1b}$), and the total rate constants k ($k_1 = k_{1a} + k_{1b}$), $CH_3OCH_2CH_3 + NO_3$ ($k_{2a}$, $k_{2b}$, $k_{2c}$, $k_{3a}$, $k_{3b}$, $k_{3c}$, $k_{4a}$, and $k_{4b}$), and the total rate constants k ($k_2 = k_{2a} + k_{2b} + k_{2c} + k_{3a} + k_{3b} + k_{3c} + k_{4a} + k_{4b}$), which are received at the CCSD(T)//BHandHLYP/6-311G(d,p)level together with the experiment data as the function of $10^3$ for *k*.

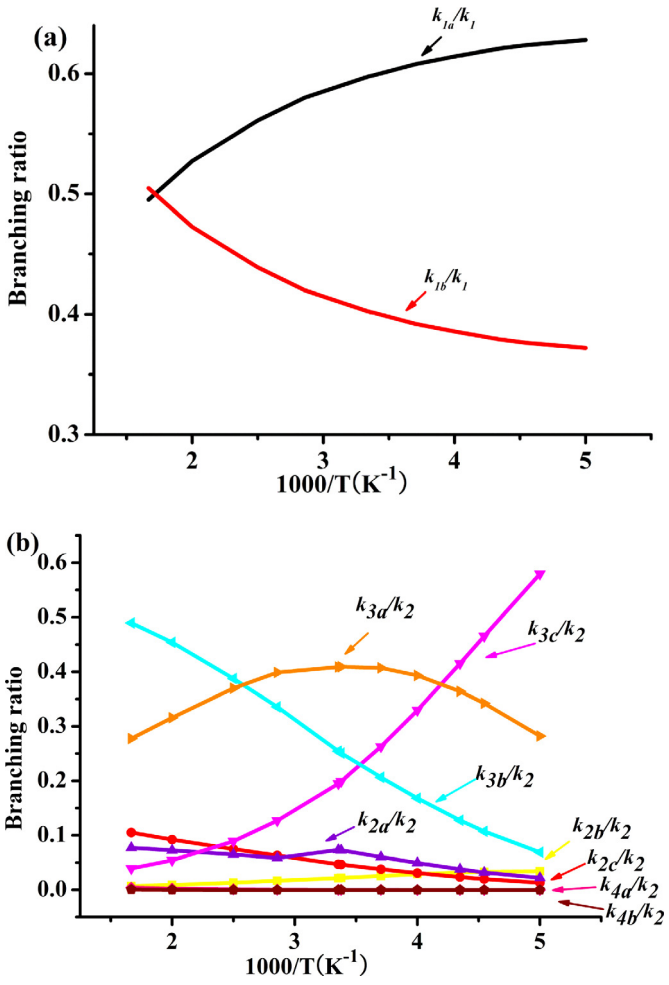


**Fig. 7.** Calculated branching ratios for reactions $CH_3OCH_3/CH_3OCH_2CH_3 + NO_3$ as a function of $10^3/T$ at the CCSD(T)//BHandHLYP/6-311G(d,p) level. (a) For reaction R1, (b) For reactions R2-4.

are competitive and should be taken into account over the whole temperature range. For example, $k_{3c}/k_2$ ratios are 0.58 at 200 K and 0.42 at 230 K. However, as the temperature increases, channel R3a should be considered and become the most competitive path. For example, the $k_{3a}/k_2$ value (0.39) large than the $k_{3c}/k_2$ value (0.33) at 250 K. Upon raising the temperature, the $k_{3a}/k_2$ value (0.40 at 350 K) is higher than the $k_{3b}/k_2$ value (0.34 at 350 K). Path R3b becomes feasible channel when temperature increases from 400 K to 600 K. For the reaction of $CH_3OCH_2CH_3$ with $NO_3$, the channels from the α–$CH_2$ group are dominant, leading to the same main products $CH_3OCHCH_3$ and $HNO_3$. However, the contribution from the α-$CH_3$ and $\beta$-$CH_3$ sites is less than 10% over whole temperature.

### 3.6. Atmospheric lifetimes

As the $NO_3$ radicals are important oxidants in the atmosphere at night, the night-time tropospheric lifetimes ($\tau$) of $CH_3OCH_3$ and $CH_3OCH_2CH_3$ was calculated according to the following equation:

$$\tau_{NO_3} = (k(NO_3) \times [NO_3])^{-1} \quad (8)$$

Using the total rate constants $8.61 \times 10^{-17}$ cm$^3$ molecule$^{-1}$ s$^{-1}$ for the reaction of $CH_3OCH_3 + NO_3$ and $7.99 \times 10^{-16}$ cm$^3$ molecule$^{-1}$ s$^{-1}$ for the reaction of $CH_3OCH_2CH_3 + NO_3$ at 298 K and the 24-h average concentration of $NO_3$ radicals ($5 \times 10^8$ molecule cm$^{-3}$) in the troposphere [51,52], the lifetimes of $CH_3OCH_3$ and $CH_3OCH_2CH_3$ are estimated to be 270 and 29 days, respectively. However, no literature reports these experimentally for comparison of the tropospheric lifetimes of $CH_3OCH_3$ and $CH_3OCH_2CH_3$ and this present investigation may set a foundation for future experimental studies.

Since there is few data available at higher temperatures, for convenience of future experimental measurements, the expression of three-parameter based on the CVT/SCT rate constants for the title reactions at the CCSD(T)//BHandHLYP/6-311G(d,p) level within 200–600 K is presented below (in cm$^3$ molecule$^{-1}$ s$^{-1}$):

$$k_1 = 1.54 \times 10^{-23} T^{3.34} \exp(-1035.53/T)$$

$$k_2 = 3.55 \times 10^{-26} T^{4.31} \exp(-281.24/T)$$

## 4. Conclusions

In this present work, theoretical kinetic study of the reactions of $NO_3$ radicals with $CH_3OCH_3$ and $CH_3OCH_2CH_3$ is investigated using variational transition state theory with small tunneling correction. The energy information is performed at the CCSD(T)//BHandHLYP/6-311G(d,p) level of theory. It is shown that each H-abstraction reaction channel (R1, R2, R3, and R4) can proceed by regioselectivity of oxygen atom (3O) of the $NO_3$ radical with $CH_3OCH_3$ and $CH_3OCH_2CH_3$ molecules. Based on energies and kinetics analysis, the attack of $NO_3$ radical occurs predominately at the α-$CH_2$ region than

α-$CH_3$, and β-$CH_3$ sites, and the C—H bond dissociation energies of the $CH_3OCH_2CH_3$ molecule are further ascertained. The model equations $k_1 = 1.54 \times 10^{-23} T^{3.34} \exp(-1035.53/T)$ and $k_2 = 3.55 \times 10^{-26} T^{4.31} \exp(-281.24/T)$ $cm^3$ $molecule^{-1}$ $s^{-1}$ have been derived within 200–600 K. In addition, the lifetimes for $CH_3OCH_3$ and $CH_3OCH_2CH_3$ are respectively obtained to be 270 and 29 days, indicating that the influence of $NO_3$ radical on these two ethers is significant in the nighttime. We hope the present theoretical studies may be helpful for estimating the kinetics of the title reactions over a wide temperature range where no experimental data are available.

## Acknowledgments

The authors thank Professor Donald G. Truhlar for providing the Polyrate, Version 9.7 program. We are grateful to financial support from Natural Science Foundation of China (No. 21377021).

## References

[1] H. Singh, Y. Chen, A. Staudt, D. Jacob, D. Blake, B. Heikes, J. Snow, Evidence from the Pacific troposphere for large global sources of oxygenated organic compounds, Nature 410 (2001) 1078–1081.
[2] G. König, M. Brunda, H. Puxbaum, C.N. Hewitt, S.C. Duckham, J. Rudolph, Relative contribution of oxygenated hydrocarbons to the total biogenic voc emissions of selected mid-European agricultural and natural plant species, Atmos. Environ. 29 (1995) 861–874.
[3] K.A. McKinney, B.H. Lee, A. Vasta, T.V. Pho, J.W. Munger, Emissions of isoprenoids and oxygenated biogenic volatile organic compounds from a New England mixed forest, Atmos. Chem. Phys. 11 (2011) 4807–4831.
[4] N. Yassaa, P. Ciccioli, E. Brancaleoni, M. Frattoni, B.Y. Meklati, Ambient measurements of selected VOCs in populated and remote sites of the Sahara desert, Atmos. Res. 100 (2011) 141–146.
[5] R. Kamens, D. Bell, A. Dietrich, J. Perry, R. Goodman, L. Claxton, S. Tejada, Mutagenic transformations of dilute wood smoke systems in the presence of ozone and nitrogen dioxide. Analysis of selected high-pressure liquid chromatography fractions from wood smoke particle extracts, Environ. Sci. Technol. 19 (1985) 63–69.
[6] T.J. Wallington, W.F. Schneider, J. Sehested, M. Bilde, J. Platz, O.J. Nielsen, L.K. Christensen, M.J. Molina, L.T. Molina, P.W. Wooldridge, Atmospheric chemistry of HFE-7100 ($C_4F_9OCH_3$): reaction with OH radicals, UV spectra and kinetic data for $C_4F_9OCH_2$‘ and $C_4F_9OCH_2O_2$‘ radicals, and the atmospheric fate of $C_4F_9OCH_2O$‘ radicals, J. Phys. Chem. A 101 (1997) 8264–8274.
[7] R. Atkinson, Gas-phase tropospheric chemistry of organic compounds: a review, Atmos. Environ. 41 (2007) 200–240.
[8] S.S. Brown, J. Stutz, Nighttime radical observations and chemistry, Chem. Soc. Rev. 41 (2012) 6405–6447.
[9] M. Glasius, A. Calogirou, N.R. Jensen, J. Hjorth, C.J. Nielsen, Kinetic study of gasphase reactions of pinonaldehyde and structurally related compounds, Int. J. Chem. Kinet. 29 (1997) 527–533.
[10] B. D'Anna, V. Bakken, J.A. Beukes, C.J. Nielsen, K. Brudnik, J.T. Jodkowski, Experimental and theoretical studies of gas phase NO3 and OH radical reactions with formaldehyde, acetaldehyde and their isotopomers, Phys. Chem. Chem. Phys. 5 (2003) 1790–1805.
[11] A.G. Russell, B. Brunekeef, A focus on particulate matter and health, Environ. Sci. Technol. 43 (2009) 4620–4625.
[12] A. Sorooshian, J. Csavina, T. Shingler, S. Dey, F.J. Brechtel, A.E. Saez, E.A. Betterton, Hygroscopic and chemical properties of aerosols collected near a copper smelter: implications for public and environmental health, Environ. Sci. Technol. 46 (2012) 9473–9480.
[13] S. Langer, E. Ljungström, Rates of reaction between the nitrate radical and some aliphatic ethers, Int. J. Chem. Kinet. 26 (1994) 367–380.
[14] L. Chen, T. Uchimaru, S. Kutsuna, K. Tokuhashi, A. Sekiya, H. Okamoto, Kinetics of gas-phase reactions of $CH_3OCH_2CF_3$, $CH_3OCH_3$, $CH_3OCH_2CH_3$, $CH_3CH_2OCH_2CH_3$, and $CHF_2CF_2OCH_2CF_3$ with $NO_3$ radicals at 298 K, Int. J. Chem. Kinet. 41 (2009) 490–497.
[15] Y.Y. Chuang, J.C. Corchado, D.C. Truhlar, Mapped interpolation scheme for single-point energy corrections in reaction rate calculations and a critical evaluation of dual-level reaction path dynamics methods, J. Phys. Chem. A 103 (1999) 1140–1149.
[16] J.Y. Wu, J.Y. Liu, Z.S. Li, C.C. Sun, Dual-level direct dynamics studies for the reactions of $CH_3OCH_3$ and $CF_3OCH_3$ with the OH radical, J. Chem. Phys. 118 (2003) 10986–10995.
[17] L. Yang, J.L. Liu, L. Wang, H.Q. He, Y. Wang, Z.S. Li, Theoretical study of the reactions $CF_3CH_2OCHF_2$ + OH/Cl and its product radicals and parent ether ($CH_3CH_2OCH_3$) with OH, J. Comput. Chem. 29 (2008) 550–561.
[18] Y.M. Ma, K.H. Su, J. Zhang, Y. Wang, X. Wang, Y. Liu, Hydrogen abstraction mechanisms and reaction rates of toluene + $NO_3$, J. Mol. Model. 21 (2015) 207.
[19] A.D. Becke, Density-functional thermochemistry. III. The role of exact exchange, J. Chem. Phys. 98 (1993) 1372–1377.
[20] M.J. Frisch, G.W. Trucks, H.B. Schlegel, G. E.Scuseria, M.A. Robb, J.R. Cheeseman, G. Scalmani, V. Barone, B. Mennucci, G.A. Petersson, H. Nakatsuji, M. Caricato, X. Li, H.P. Hratchian, A.F. Izmaylov, J. Bloino, G. Zheng, J.L. Sonnenberg, M. Hada, M. Ehara, K. Toyota, R. Fukuda, J. Hasegawa, M. Ishida, T. Nakajima, Y. Honda, O. Kitao, H. Nakai, T. Vreven, J.A. Montgomery Jr., J.E. Peralta, F. Ogliaro, M. Bearpark, J.J. Heyd, E. Brothers, K.N. Kudin, V.N. Staroverov, Kobayashi, J. Normand, K. Raghavachari, A. Rendell, J.C. Burant, S.S. Iyengar, J. Tomasi, M. Cossi, N. Rega, N.J. Millam, M. Klene, J.E. Knox, J.B. Cross, V. Bakken, C. Adamo, J. Jaramillo, R. Gomperts, R.E. Stratmann, O. Yazyev, A.J. Austin, R. Cammi, C. Pomelli, J.W. Ochterski, R.L. Martin, K. Morokuma, V.G. Zakrzewski, G.A. Voth, P. Salvador, J.J. Dannenberg, S. Dapprich, A.D. Daniels, O. Farkas, J. Foresman, J.V. Ortiz, J. Cioslowski, D.J. Fox, Gaussian09, Revision B.01, Gaussian, Inc, Wallingford, 2010.
[21] J.M. Anglada, S. Olivellaa, A. Solé, Atmospheric formation of the $NO_3$ radical from gas-phase reaction of $HNO_3$ acid with the $NH_2$ radical: proton-coupled electron-transfer versus hydrogen atom transfer mechanisms, Phys. Chem. Chem. Phys. 16 (2014) 19437–19445.
[22] A.M. El-Nahas, T. Uchimaru, M. Sugie, K. Tokuhashi, A. Sekiya, Hydrogen abstraction from dimethyl ether (DME) and dimethyl sulfide (DMS) by OH radical: a computational study, J. Mol. Struct. (THEOCHEM) 722 (2005) 9–19.
[23] T. Uchimaru, S. Tsuzuki, M. Sugie, K. Tokuhashi, A. Sekiya, A theoretical study on the strength of two-center three-electron bonds in the $NO_3$ radical adducts of reduced sulfur molecules, $H_2S$ $CH_3SH$, $CH_3SCH_3$, and $CH_3SSCH_3$, Chem. Phys. 324 (2006) 465–473.
[24] M.Q. Huang, Y.M. Liao, Z.Y. Wang, L.Q. Hao, W.J. Zhang, A theoretical investigation of $NO_3$-initiated oxidation of toluene, Comput. Theor. Chem. 1037 (2014) 63–69.
[25] K. Raghavachari, G.W. Trucks, J.A. Pople, M.A. Head-Gordon, A fifth-order perturbation comparison of electron correlation theories, Chem. Phys. Lett. 157 (1989) 479–483.
[26] J.C. Rienstra-Kiracofe, W.D. Allen, H.F. Schaefer, The $C_2H_5$+$O_2$ reaction mechanism: high-level ab initio characterizations, J. Phys. Chem. A 104 (2000) 9823–9840.
[27] A. Galano, L. Muñoz-Rugeles, J.R. Alvarez-Idaboy, J.L. Bao, D.G. Truhlar, Hydrogen abstraction reactions from phenolic compounds by peroxyl radicals: multireference character and density functional theory rate constants, J. Phys. Chem. A 120 (2016) 4634–4642.
[28] J.C. Corchado, Y.Y. Chuang, P.L. Fast, W.P. Hu, Y.P. Liu, G.C. Lynch, K.A. Nguyen, C.F. Jackels, A. Fernandez-Ramosand, B.A. Ellingson, et al., POLYRATE, Version 9.7, University of Minnesota, Minneapolis, MN, 2007.
[29] B.C. Garrett, D.G. Truhlar, Generalized transition state theory. Bond energy-bond order method for canonical variational calculations with application to hydrogen atom transfer reactions, J. Am. Chem. Soc. 101 (1979) 4534–4548.
[30] B.C. Garrett, D.G. Truhlar, R.S. Grev, A.W. Magnuson, Improved treatment of threshold contributions in variational transition-state theory, J. Phys. Chem. 84 (1980) 1730–1748.
[31] Y.P. Liu, G.C. Lynch, T.N. Truong, D.H. Lu, D.G. Truhlar, B.C. Garrett, Molecular modeling of the kinetic isotope effect for the [1,5]-sigmatropic rearrangement of cis-1,3-pentadiene, J. Am. Chem. Soc. 115 (1993) 2408–2415.
[32] D.H. Lu, T.N. Truong, V.S. Melissas, G.C. Lynch, Y.P. Liu, B.C. Grarrett, R. Steckler, A.D. Issacson, S.N. Rai, G.C. Hancock, J.G. Lauderdale, T. Joseph, D.G. Truhlar, A new version of a computer program for the calculation of chemical reaction rates for polyatomics, Comput. Phys. Commun. 71 (1992) 235–262.
[33] T. Shimanouchi, Tables of Molecular Vibrational Frequencies Consolidated Volume I NSRDSNBS 39, U.S. Govt. Printing Office, Washington, 1972.
[34] B. Kim, P.L. Hunter, H.S. Johnston, $NO_3$ radical studied by laser-induced fluorescence, J. Chem. Phys. 96 (1992) 4057.
[35] A. Weaver, S.E. Bradforth, D.W. Arnold, D.M. Neumark, Examination of the $2A'_2$ and 2E states of $NO_3$ by ultraviolet photoelectron spectroscopy of $NO^-_3$, J. Chem. Phys. 94 (1991) 1740–1751.
[36] X.B. Wang, W. Yang, L.S. Wang, Photodetachment and theoretical study of free and water-solvated nitrate anions, $NO^-_3(H_2O)n$ (n = 0–6), J. Chem. Phys. 116 (2002) 561–570.
[37] I.S. Ignatyev, Y.M. Xie, W.D. Allen, H.F. Schaefer, Mechanism of the $C_2H_5 + O_2$ reaction, J. Chem. Phys. 107 (1997) 141–155.
[38] H.B. Schlegel, C. Sosa, Ab initio molecular orbital calculations on $F + H_2 \rightarrow HF + H$ and $OH + H_2 \rightarrow H_2O + H$ using unrestricted Møller-Plesset perturbation theory with spin projection, Chem. Phys. Lett. 145 (1988) 329–333.
[39] C.D. Sherrill, M.S. Lee, M. Head-Gordon, Chem. Phys. Lett. 302 (1999) 425–430.
[40] G.S. Hammond, A correlation of reaction rates, J. Am. Chem. Soc. 77 (1955) 334–338.
[41] B.K. Mishra, M. Lily, A.K. Chakrabartty, R.C. Deka, A.K. Chandra, A DFT study on kinetics of the gas phase reactions of $CH_3CH_2OCF_3$ with OH radicals and Cl atoms, J. Fluor. Chem. 159 (2014) 57–64.
[42] F.Y. Bai, Y.J. Liu, X. Wang, Y.Q. Sun, X.M. Pan, Atmospheric chemistry of CF3(CX2)2CH2OH: rate coefficients and temperature dependence of reactions with chlorine atoms and the subsequent pathways of alkyl and alkoxy radicals (X = H F), RSC. Adv. 6 (2016) 63954–63964.
[43] J.R. Alvarez-Idaboy, A. Galano, G. Bravo-Peírez, M.E. Ruiz, Rate constant dependence on the size of aldehydes in the $NO_3$ + Aldehydes reaction. An explanation via quantum chemical calculations and CTST, J. Am. Chem. Soc. 123 (2001) 8387–8395.

[44] J.R. Alvarez-Idaboy, N. Mora-Diez, A. Vivier-Bunge, A quantum chemical and classical transition state theory explanation of negative activation energies in OH addition to substituted ethenes, J. Am. Chem. Soc. 122 (2000) 3715–3720.
[45] A. Galano, J.R. Alvarez-Idaboy, G. Bravo-Peírez, M.E. Ruiz-Santoyo, Gas phase reactions of C1-C4 alcohols with the OH radical: a quantum mechanical approach, Phys. Chem. Chem. Phys. 4 (2002) 4648–4662.
[46] J.R. Alvarez-Idaboy, L. Reyes, N. Mora-Diez, The mechanism of the Baeyer-Villiger rearrangement: quantum chemistry and TST study supported by experimental kinetic data, Org. Biomol. Chem. 5 (2007) 3682–3689.
[47] D.L. Singleton, R.J. Cvetanovic, Temperature dependence of the reactions of oxygen atoms with Olefins1, J. Am. Chem. Soc. 98 (1976) 6812.
[48] A. Galano, J.R. Alvarez-Idaboy, L.A. Montero-Cabrera, A. VivierBunge, OH hydrogen abstraction reactions from alanine and glycine: a quantum mechanical approach, J. Comput. Chem. 22 (2001) 1138–1153.
[49] A. Galano, J.R. Alvarez-Idaboy, G. Bravo-Pe'rez, M.E. Ruiz-Santoyo, Mechanism and rate coefficients of the gas phase OH hydrogen abstraction reaction from asparagine: a quantum mechanical approach, THEOCHEM 617 (2002) 77.
[50] F.Y. Bai, G. Sun, X. Wang, Y.Q. Sun, R.S. Wang, X.M. Pan, Theoretical study on the reactions of $(CF_3)_2CFOCH_3$ + OH/Cl and reaction of $(CF_3)_2CFOCHO$ with Cl atom, J. Phys. Chem. A 119 (2015) 1256–1266.
[51] T.E. Kleindienst, P.B. Shepson, E.O. Edney, L.D. Claxton, L.T. Cupitt, Wood smoke measurement of the mutagenic activities of its gas- and particulate-phase photooxidation products, Environ. Sci. Technol. 20 (1986) 493–501.
[52] M. Ezzati, D.M. Kammen, The health impacts of exposure to indoor air pollution from solid fuels in developing countries: knowledge, gaps, and data needs, Environ. Health. Perspect. 110 (2002) 1057–1068.